OXFORD CDE

Journal of Computational Design and Engineering, 2021, 8(4), 1158–1171

https://doi.org/10.1093/jcde/qwab038
Journal homepage: www.jcde.org

RESEARCH ARTICLE

Spectral relaxation computation of electroconductive nanofluid convection flow from a moving surface with radiative flux and magnetic induction

Shahina Akter[1,2], M. Ferdows[1,*], Tasveer A. Bég[3], O. Anwar Bég[4], A. Kadir[4] and Shuyu Sun[5]

[1]Research Group of Fluid Flow Modeling and Simulation, Department of Applied Mathematics, University of Dhaka, Dhaka 1000, Bangladesh; [2]Department of Computer Science and Engineering, University of Information Technology and Sciences, Dhaka 1212, Bangladesh; [3]Engineering Mechanics Research, Israfil House, Dickenson Road, Manchester M13 OYL, UK; [4]Multi-Physical Engineering Sciences Group, Mechanical Engineering Department, School of Science, Engineering and Environment (SEE), University of Salford, Maxwell Building, The Crescent, Salford M5 4WT, Manchester, UK and [5]Department of Computational and Applied Mathematics, 4700 King Abdullah University of Science and Technology, Thuwal, Makkah Province, 23955-6900, Saudi Arabia

*Corresponding author. E-mail: ferdows@du.ac.bd

Abstract

A theoretical model is developed for steady magnetohydrodynamic viscous flow resulting from a moving semi-infinite flat plate in an electrically conducting nanofluid. Thermal radiation and magnetic induction effects are included in addition to thermal convective boundary conditions. Buongiorno's two-component nanoscale model is deployed, which features Brownian motion and thermophoresis effects. The governing nonlinear boundary layer equations are converted to nonlinear ordinary differential equations by using suitable similarity transformations. The transformed system of differential equations is solved numerically, employing the spectral relaxation method (SRM) via the MATLAB R2018a software. SRM is a simple iteration scheme that does not require any evaluation of derivatives, perturbation, and linearization for solving a nonlinear system of equations. Effects of embedded parameters such as *sheet velocity parameter* λ, *magnetic field parameter* β, *Prandtl number* Pr, *magnetic Prandtl number* Prm, *thermal radiation parameter* Rd, *Lewis number* Le, *Brownian motion parameter* Nb, *and thermophoresis parameter* Nt on velocity, induced magnetic field, temperature, and nanoparticle concentration profiles are investigated. The skin-friction results, local Nusselt number, and Sherwood number are also discussed for various values of governing physical parameters. To show the convergence rate against iteration, residual error analysis has also been performed. The flow is strongly decelerated, and magnetic induction is suppressed with greater magnetic body force parameter, whereas temperature is elevated due to extra work expended as heat in dragging the magnetic nanofluid. Temperatures are also boosted with increment in nanoscale thermophoresis parameter and radiative parameter, whereas they are reduced with higher wall velocity, Brownian motion, and Prandtl numbers. Both hydrodynamic and magnetic boundary layer thicknesses are reduced with greater reciprocal values of the magnetic Prandtl number Pr_m. Nanoparticle (concentration) boundary layer thickness is boosted with higher values of thermophoresis and

Received: 13 February 2021; **Revised:** 3 June 2021; **Accepted:** 4 June 2021

© The Author(s) 2021. Published by Oxford University Press on behalf of the Society for Computational Design and Engineering. This is an Open Access article distributed under the terms of the Creative Commons Attribution License (http://creativecommons.org/licenses/by/4.0/), which permits unrestricted reuse, distribution, and reproduction in any medium, provided the original work is properly cited.

Downloaded from https://academic.oup.com/jcde/article/8/4/1158/6324282 by University of Salford user on 29 July 2021

Prandtl number, whereas it is diminished with increasing wall velocity, nanoscale Brownian motion parameter, radiative parameter, and Lewis number. The simulations are relevant to electroconductive nanomaterial processing.

Keywords: magnetic nanofluid; induction; convection; radiation; moving sheet; Buongiorno model; nanoparticle diffusion; spectral relaxation method (SRM); MATLAB

Notation

Roman:

C_f :	Skin-friction coefficient
C_w :	Nanoparticle concentration at the moving wall
C_∞ :	Nanoparticle concentration in the free stream
D :	Differentiation matrix in spectral algorithm
D_T :	Buongiorno nanoscale thermophoresis diffusion coefficient
D_B :	Buongiorno nanoscale Brownian diffusion coefficient
f:	Dimensionless stream function
f :	Vector function at the collocation points
f′ :	Dimensionless velocity
g:	Dimensionless magnetic induction stream function
g′ :	Dimensionless induced magnetic field stream function gradient
$F_{r+1}(\eta)$:	Current iteration level of dimensionless velocity
$G_{r+1}(\eta)$):	Current iteration level of dimensionless magnetic stream function
H_1, H_2 :	Dimensional magnetic stream function components
K:	Thermal conductivity of magnetic nanofluid
K_S:	Radiative mean absorption coefficient
Le :	Lewis number
N:	Collocation points deployed in spectral method
Nu_x :	Local Nusselt number
O :	Size of the matrix in spectral algorithm
Pr :	Prandtl number
Pr_m:	Magnetic Prandtl number
q_m :	Nanoparticle mass transfer rate at the wall
q_r :	Fourier heat flux
q_w :	Heat transfer rate at the wall
Rd :	Radiation parameter (Rosseland number)
Re_x :	Local Reynolds number
Sh_x:	Local Sherwood number
T:	Magnetic nanofluid temperature
T_w :	Temperature at the moving wall
T_∞ :	Temperature in the free stream
U :	Velocity of the free stream (at boundary layer edge)
U_w :	Velocity of moving wall (sheet)
u, v:	Dimensional velocity components along the *x*-axis and *y*-axis, respectively

Greek:

α :	Thermal diffusivity of the nanofluid
α_1 :	Magnetic diffusivity of nanofluid
B :	Magnetic body force number
λ :	Moving wall velocity parameter
η :	Dimensionless similarity variable (transverse coordinate)
η_∞ :	Infinity value (to edge of boundary layer domain)
ρ :	Magnetic nanofluid density
$(\rho C_p)_f$:	Heat capacity of the base fluid
$\sigma*$:	Stefan–Boltzmann constant
θ:	Dimensionless temperature function
φ :	Dimensionless nanoparticle concentration function
μ:	Magnetic nanofluid dynamic viscosity
ν :	Magnetic nanofluid kinematic viscosity
μ_0 :	Magnetic nanofluid permeability
τ :	Heat capacity of the magnetic nanoparticles.
τ_j :	Gauss–Lobatto collocation points
τ_w :	Shear stress at the wall
ψ :	Dimensional stream function
Φ :	Dimensional magnetic stream function

1. Introduction

Nanoscale colloidal suspensions containing solid nanoparticles and fibers are called *nanofluids* and were first introduced by Choi (1995). Choi *et al.* (2001) showed that the addition of a small number of nanoparticles to conventional heat transfer liquids such as water, toluene, oil and ethylene glycol, etc. enhances the thermal conductivity of the original fluids. In recent years, much interest has been given to the study of nanofluids owing to their greatly enhanced thermal conductivity properties (Keblinski *et al.*, 2005). A large number of numerical and experimental studies have been carried out by numerous researchers on thermal conductivity, thermal diffusivity, viscosity, and convective heat transfer characteristics of nanofluids (Choi *et al.*, 2004; Liu *et al.*, 2005; Maiga *et al.*, 2005; Das *et al.*, 2006, 2007; Kang *et al.*, 2006; Tyler *et al.*, 2006; Tiwari & Das, 2007; Abu-Nada, 2008; Oztop & Abu-Nada, 2008; Tzou, 2008; Yu *et al.*, 2008; Choi, 2009). Nanoparticles can help to extract energy from the core of the earth, improve the efficiency of the cooling system employed in nuclear reactors, and can also help in targeted drag delivery in pharmaceutics. An exquisite collection of published works on nanofluids is given by Das *et al.* (2007), and comprehensive references are also provided in the review papers of Wang and Mujumdar (2007, 2008a, b).

Magnetohydrodynamics (MHD) is the study of the motion of electrically conducting fluids with magnetic properties. These include both inviscid and viscous fluids. A current induced in the presence of a magnetic field in an electrically conducting fluid polarizes the liquid, and as a result, the magnetic field also changes. The fluids can be conducting electrically in various applications for the processing of materials in chemical and mechanical engineering, and as such, they will react to an applied magnetic field. Such a system may be used to monitor, e.g. the heat transfer levels on stretch sheets, and to fine-tune the final materials to industry requirements. This process takes advantage of the effect of the Lorentzian drag force that abates flows in a perpendicular direction of the magnetic field applied (transverse) (Hughes & Young, 1966). MHD boundary layer flows also arise in MHD power generator designs, liquid metal manipulation, plasma studies, cooling of nuclear reactors, induction heating, plasma cutting, etc. Jafar *et al.* (2011) examined MHD flow and heat transfer over stretching/shrinking sheets with an external magnetic field. The effects of thermal radiation of MHD flow, free convection flow, and viscoelastic flow were analysed, respectively, by Chamkha (1997), Raptis (1998b), Jumah *et al.* (2001), and Mohammadein and El-Amin (2000). Recently, MHD boundary layer flow with heat and mass transfer of nanofluids has been given a great deal of attention by the

Downloaded from https://academic.oup.com/jcde/article/8/4/1158/6324282 by University of Salford user on 29 July 2021

researchers owing to significant thermal enhancement properties achieved by these nano-engineered liquids. Furthermore, by combining magnetic and nanofluid material properties, one can obtain magnetic nanofluids with exceptional magnetic responsive features. Magnetic actuation offers specific capabilities as it can be controlled momentarily and spatially, and can be applied externally to the device, offering a noninvasive remote control approach. The boundary layer flow of nanofluids over a moving surface in a flowing fluid was investigated by Bachok *et al.* (2010). Ferdows *et al.* (2012) studied the steady 2D flow of an incompressible viscous and electrically conducting nanofluid generated by a stretching sheet in the vertical direction with viscous dissipation in saturated porous media. Unsteady boundary layer flows of nanofluids from a stretching sheet with thermal radiation in the presence of a magnetic field were numerically addressed by Ferdows *et al.* (2012). Mabood *et al.* (2015) and Mustafa *et al.* (2015) studied MHD flow and nanofluid heat transfer due to a nonlinear stretching sheet. Srinivasacharya *et al.* (2015) investigated the steady laminar MHD nanofluid flow over a wedge in the presence of a variable magnetic field. MHD boundary layer flow of nanofluid over a continuously stretching surface was studied by Rasheed *et al.* (2017). Yohannes and Shankar (2014) successfully analysed melting heat transfer in nanofluid's MHD flow over a permeable exponentially stretching sheet. The behavior of nanofluid and heat and mass transfer of free convective MHD of Ag–Kerosene oil nanofluid was elucidated by Upreti *et al.* (2020). The obtained results showed that the heat and mass transfer rates grew consistently as the quantity of surface mass flux shifted from injection to suction domain. Nadeem *et al.* (2019) analysed the characteristics of heat and mass transfer for the three-dimensional unsteady, laminar, and an incompressible flow of a micropolar nanofluid.

Free convection flow of a nanofluid in the presence of a magnetic field from a vertical semi-infinite flat plate was investigated by Hamad *et al.* (2011). The impact of thermophoresis and Brownian motion in heat transfer enhancement in natural convection of nanofluids was examined by Haddad *et al.* (2012). Daniel *et al.* (2018) studied the combined effects of thermal stratification, applied magnetic field, and thermal radiation on a boundary layer flow of electrically conducting nanofluid over a nonlinear stretching sheet. The radiative heat transfer is found sensitive to an increase in the fluid temperature and thicker thermal boundary layer thickness. Das *et al.* (2016) studied the impact of thermophoresis and thermal radiation on heat and mass transfer for the second-grade fluid flow passing through a semi-infinite stretching sheet with convective surface heat flux and explored that the fluid velocity and temperature in the boundary layer region rise significantly for increasing the values of thermal radiation parameter.

The above studies did not consider magnetic induction effects, which become significant at higher magnetic Reynolds numbers, e.g. MHD nanomaterials processing (Bég *et al.*, 2014; Aly & Sayed, 2017). Additionally, in high-temperature nanomaterial processing, thermal radiation is significant. Mathematical models of magnetic nanoliquid fabrication processes therefore require radiative heat flux to be also incorporated, as elaborated in several recent studies (Ferdows *et al.*, 2014; Uddin *et al.*, 2015; Madkour, 2019). *In this work, thus, a new model is presented for MHD induction convection flow of an electrically conducting nanofluid from a moving semi-infinite stretching surface with appreciable thermal radiative heat transfer.* This constitutes the novelty of the present simulations, which for the first time use a spectral relaxation method (SRM) and combine properly electromagnetic induction, moving sheet velocity effects, nonlinear radiative flux

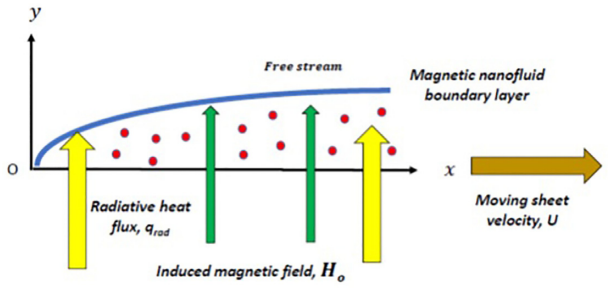

Figure 1: Magnetic induction nanofluid radiative convection physical model.

(for high-temperature material processing), and heat and mass transfer via the Buongiorno model. The Rosseland diffusion flux model is deployed for optically thick magnetic nanofluids (Khan *et al.*, 2013; Bég *et al.*, 2014). Using suitable similarity transformations, the momentum and energy equations are converted into dimensionless coupled ordinary differential equations and solved with a numerical technique known as the SRM (Bég *et al.*, 2014, 2016; Haroun *et al.*, 2015). Validation with the earlier study of Shateyi and Prakash (2014) is included. The effects of embedded parameters, i.e. moving sheet velocity parameter λ, magnetic field parameter β, Prandtl number Pr, magnetic Prandtl number Prm, thermal radiation parameter Rd, Lewis number Le, Brownian motion parameter Nb and thermophoresis parameter Nt on velocity, induced magnetic field, temperature, nanoparticle concentration, skin friction, local Nusselt number, and Sherwood number profiles, are visualized. A residual error analysis is included for the convergence rate against iteration. The simulations are relevant to multiphysical magnetic nanoliquid material processing (Ali *et al.*, 2018).

2. Governing Equations for Magnetic Induction Nanofluid Flow

Consider the 2D, steady, viscous MHD thermal convection boundary layer flow of an electrically conducting nanofluid from a moving semi-infinite surface (sheet). The physical model is shown in Fig. 1. A uniform magnetic field of force H_0 is applied to the surface in the normal direction. In contrast, the normal component of the induced magnetic field H_2 disappears when it hits the wall and the parallel component H_1 approaches the value of H_0.

It is also assumed that the velocity of the free stream is *U*, and that of the plate (sheet) is $U_w = \lambda U$, where λ is a velocity parameter. Maxwell displacement current, Hall current, viscous and Ohmic dissipation, and also chemical reaction effects are neglected. At the moving surface, the temperature and the nanoparticle concentration take constant values T_w and C_w, respectively, while the free stream values are prescribed as T_∞ and C_∞, respectively. Under the boundary layer approximations, using the Buongiorno two-component nanoscale model (Buongiorno, 2006) [as elaborated in detail by Bég (2018)] and the Rosseland diffusion flux model for radiative transfer (Bég *et al.*, 2014; Ferdows *et al.*, 2014; Uddin *et al.*, 2015), the conservation equations can be written as follows:

$$\frac{\partial u}{\partial x} + \frac{\partial v}{\partial y} = 0, \tag{1}$$

$$\frac{\partial H_1}{\partial x} + \frac{\partial H_2}{\partial y} = 0, \tag{2}$$

$$u\frac{\partial u}{\partial x} + v\frac{\partial u}{\partial y} = \nu\frac{\partial^2 u}{\partial y^2} + \frac{\mu_0}{\rho}\left(H_1\frac{\partial H_1}{\partial x} + H_2\frac{\partial H_1}{\partial y}\right), \tag{3}$$

Downloaded from https://academic.oup.com/jcde/article/8/4/1158/6324282 by University of Salford user on 29 July 2021

$$u\frac{\partial H_1}{\partial x}+v\frac{\partial H_1}{\partial y}-H_1\frac{\partial u}{\partial x}-H_2\frac{\partial u}{\partial y}=\alpha_1\frac{\partial^2 H_1}{\partial y^2}, \tag{4}$$

$$u\frac{\partial T}{\partial x}+v\frac{\partial T}{\partial y}=\alpha\frac{\partial^2 T}{\partial y^2}-\frac{\alpha}{K}\frac{\partial q_r}{\partial y}+\tau\left[D_B\frac{\partial C}{\partial y}\frac{\partial T}{\partial y}+\left(\frac{D_T}{T_\infty}\right)\left(\frac{\partial T}{\partial y}\right)^2\right], \tag{5}$$

$$u\frac{\partial C}{\partial x}+v\frac{\partial C}{\partial y}=D_B\frac{\partial^2 C}{\partial y^2}+\frac{D_B}{T_\infty}\frac{\partial^2 T}{\partial y^2}, \tag{6}$$

where u and v are the velocity components along the x-axis and the y-axis, respectively, T is the nanofluid temperature, ρ and ν are the nanofluid density and kinematic viscosity coefficient, respectively, μ_0 is the magnetic permeability, α_1 is the magnetic diffusivity, $\alpha=\frac{K}{(\rho C_p)_f}$ is the thermal diffusivity of the fluid, K is the thermal conductivity of magnetic nanofluid, $(\rho C_p)_f$ is the heat capacity of the base fluid, q_r is the heat flux, D_B is the Brownian diffusion coefficient, D_T is the thermophoresis diffusion coefficient, $\tau=\frac{(\rho C_p)_p}{(\rho C_p)_f}$, and $(\rho C_p)_p$ is the heat capacity of the nanoparticles.

The radiative heat flux q_r is evaluated by using Rosseland diffusion approximation (Hossain & Takhar, 1996) and following Raptis (1998a) among other researchers, to be

$$q_r=\frac{4\sigma^*}{3K_s}\frac{\partial T^4}{\partial y}, \tag{7}$$

where σ^* and K_s are the Stephan–Boltzman constant and the Rosseland mean absorption coefficient, respectively. The temperature differences within the flow are sufficiently small under the assumption that T^4 may be expressed as a linear combination of the temperature as shown in Chamakha (1997). Expanding T^4 in a Taylor series about T_∞ and neglecting the higher order terms, we obtain

$$T^4\cong 4T_\infty^3T-3T_\infty^4. \tag{8}$$

Using (7) and (8) in equation (5), we obtain

$$\frac{\partial q_r}{\partial y}=-\frac{16\sigma^*T_\infty^3}{3K_s}\frac{\partial^2 T}{\partial y^2}. \tag{9}$$

The prescribed boundary conditions at the wall (plate) and in the free stream for equations (1)–(6) are defined as follows:

At $y=0$:

$$u=\lambda U,\quad v=0,\quad \frac{\partial H_1}{\partial y}=H_2=0,\quad T=T_w,\quad C=C_w, \tag{10a}$$

At $y\to\infty$:

$$u\to U,\quad H_1\to H_0,\quad T\to T_\infty,\quad C\to C_\infty. \tag{10b}$$

3. Similarity Transformations

We now introduce the following similarity transformations, to normalize the boundary layer equations:

$$\psi=(2U\nu x)^{\frac{1}{2}}f(\eta),\quad \Phi=\left(\frac{2\nu x}{U}\right)^{\frac{1}{2}}H_0\,g(\eta),\quad \eta=\left(\frac{U}{2\nu x}\right)^{\frac{1}{2}}y$$

$$\theta(\eta)=\frac{T-T_\infty}{T_w-T_\infty},\quad \varphi(\eta)=\frac{C-C_\infty}{C_w-C_\infty}. \tag{11}$$

Here, ψ is the stream function, which is defined as $u=\frac{\partial\psi}{\partial y}$ and $v=-\frac{\partial\psi}{\partial x}$, and Φ is the magnetic stream function, defined by $H_1=\frac{\partial\Phi}{\partial y}$ and $H_2=-\frac{\partial\Phi}{\partial x}$. Furthermore, η is the dimensionless similarity variable (transverse coordinate), f and g are dimensionless stream and magnetic stream functions, respectively, θ is the dimensionless temperature function, and φ is the dimensionless nanoparticle concentration. Mass conservation (1) and magnetic field continuity (2) are satisfied identically. Substituting the similarity variables into equations (3)–(6) gives the following similarity ordinary nonlinear differential momentum, magnetic, thermal, and species (nanoparticle) boundary layer equations:

$$f'''+ff''-\beta g\,g''=0, \tag{12}$$

$$\frac{1}{Prm}g'''+fg''-g\,f''=0, \tag{13}$$

$$\left(\frac{3+4Rd}{Pr}\right)\theta''+f\theta'+Nb\theta'\varphi'+Nt\,\theta'^2=0, \tag{14}$$

$$\varphi''+Lef\varphi'+\frac{Nt}{Nb}\theta''=0. \tag{15}$$

The dimensionless boundary conditions for the tenth-order problem now become

$$f(0)=0,f'(0)=\lambda,\ g(0)=g''(0)=0,$$

$$\theta(0)=1,\ \varphi(0)=1\ \text{as}\ \eta=0 \tag{16a}$$

$$f'\to 1,\ g'\to 1,\ \theta\to 0,\ \varphi\to 0\ \text{as}\ \eta\to\infty. \tag{16b}$$

Here, primes denote differentiation with respect to η, f' is the dimensionless velocity, g' is the dimensionless induced magnetic field stream function gradient, $Pr=\frac{\nu}{\alpha}$ is the Prandtl number, $Pr_m=\frac{\nu}{\alpha_1}$ is the magnetic Prandtl number, $\beta=\frac{\mu_0H_0^2}{\rho U^2}$ is the magnetic body force number, $Rd=\frac{4\sigma^*T_\infty^3}{KK_s}$ is the radiation parameter, $Nb=\frac{\tau D_B}{\nu}(C_w-C_\infty)$ is the Brownian motion parameter, $Nt=\frac{\tau D_T}{\nu T_\infty}(T_w-T_\infty)$ is the thermophoresis parameter, and $Le=\frac{\nu}{D_B}$ is the Lewis number. The physical quantities of interest in magnetic material processing are the skin-friction coefficient C_f, the local Nusselt number Nu_x, and the local Sherwood number Sh_x. These parameters, respectively, characterize the surface drag, wall heat transfer rate, and wall nanoparticle mass transfer rate. The skin-friction coefficient is defined as

$$C_f=\frac{\tau_w}{\rho U^2}. \tag{17}$$

Here, τ_w is the shear stress at the surface of the wall (sheet), which is given by

$$\tau_w=\mu\left[\frac{\partial u}{\partial y}\right]_{y=0}=\rho U^{\frac{3}{2}}\sqrt{\frac{\nu}{2x}}f''(0). \tag{18}$$

Using equation (18) in (17), we obtain the dimensionless skin-friction coefficient (surface drag) as

$$\sqrt{2Re_x}C_f=f''(0). \tag{19}$$

The Nusselt number is defined as

$$Nu_x=\frac{xq_w}{K(T_w-T_\infty)}, \tag{20}$$

where the heat transfer rate at the surface is given by

$$q_w=-K\left[\frac{\partial T}{\partial y}\right]_{y=0}=-K(T_w-T_\infty)\sqrt{\frac{U}{2\nu x}}\theta'(0). \tag{21}$$

Using equation (21) in (20), the dimensionless wall heat transfer rate is obtained as

$$\sqrt{\frac{2}{Re_x}}Nu_x=-\theta'(0). \tag{22}$$

Downloaded from https://academic.oup.com/jcde/article/8/4/1158/6324282 by University of Salford user on 29 July 2021

The nanoparticle mass transfer rate at the surface is given by

$$q_m = -D_B\left[\frac{\partial C}{\partial y}\right]_{y=0} = -D_B\,(C_w - C_\infty)\sqrt{\frac{U}{2\nu x}}\,\varphi'(0). \tag{23}$$

The Sherwood number is defined as

$$Sh_x = \frac{x q_m}{D_B\,(C_w - C_\infty)}. \tag{24}$$

From equations (23) and (24), the dimensionless nanoparticle mass transfer rate becomes

$$\sqrt{\frac{2}{Re_x}}\,Sh_x = -\varphi'(0). \tag{25}$$

Here, $Re_x = \frac{Ux}{\nu}$ is the local Reynolds number. According to Bachok *et al.* (2010), $Re_x^{-1/2}Nu_x$ and $Re_x^{-1/2}Sh_x$ are referred to as the reduced Nusselt number and reduced Sherwood number, which are represented by $-\theta'(0)$ and $-\varphi'(0)$, respectively.

4. Computational Solution with SRM

The SRM is an iterative algorithm proposed for nonlinear systems of differential equations in which some of the unknown functions have exponentially decaying profiles. The method has been identified to be very efficient and convenient in solving boundary-layer problems in which at least one of the profiles such as velocity, temperature, or concentration decays exponentially. The SRM approach is derived from importing and linearizing the Gauss–Seidel concept of decoupling a system of equations by a simple rearrangement of the order in which they are described and sequentially resolved. The resulting SRM iterative scheme is then implemented using the Chebyshev Spectral Collocation process wherein such polynomials provide good accuracy and fast convergence in the computations. This approach has been recently introduced by Motsa (2014). SRM has been applied by Motsa and Makukula (2013) to solve the swirling Von Karman disk flow of a Reiner–Rivlin fluid with Joule heating, viscous dissipation, and wall transpiration. It has also been implemented in thermal ignition flows of rheological rocket gel propellants by Awad *et al.* (2014) and in micropolar convective wall plumes in geothermic by Haroun *et al.* (2015). The SRM algorithm, when applied to the transformed equations (9)–(12), may be summarized as follows:

I. Reduce the order of the velocity and induced magnetic equations by introducing the transformation $f'(\eta) = F(\eta)$ and $g'(\eta) = G(\eta)$ and express the original equations in terms of $F(\eta)$ and $G(\eta)$.
II. The iteration scheme is developed by assuming that only linear terms in $F(\eta)$ and $G(\eta)$ are to be evaluated at the current iteration level [denoted by $F_{r+1}(\eta)$ and $G_{r+1}(\eta)$], and all other terms (linear and nonlinear) in $f(\eta)$ and $g(\eta)$ are assumed to be known from the previous iteration [denoted by $f_r(\eta)$ and $g_r(\eta)$]. Also, besides nonlinear terms in $F(\eta)$ and $G(\eta)$ are also calculated at the previous iteration.
III. The process is repeated for the other governing variables using the updated solutions of the variables determined in the previous equation.

The strategy stated above for decoupling a linear algebraic system of equations is analogous to the Gauss–Seidel relaxation method. Applying this algorithm leads to a series of linear differential equations with variable coefficients that are solved here using Chebyshev spectral collocation methods (Awad *et al.*, 2014; Haroun *et al.*, 2015). Due to their noticeable high precision and relative efficiency, spectral methods are used here in discretizing and for the subsequent solution of variable coefficient linear differential equations with smooth solutions over a simple domain. To apply the SRM to the nonlinear ordinary differential equations, we define $f'(\eta) = F(\eta)$ and $g'(\eta) = G(\eta)$ and then orchestrate the problem as the following set of equations:

$$f' = F, \tag{26}$$

$$F'' + fF' - \beta g\,G' = 0, \tag{27}$$

$$g' = G, \tag{28}$$

$$\frac{1}{Prm}G'' + fG' - g\,G' = 0, \tag{29}$$

$$\frac{1+Rd}{Pr}\theta'' + f\theta' + Nb\theta'\varphi' + Nt\,\theta'^2 = 0, \tag{30}$$

$$\varphi'' + Lef\varphi' + \frac{Nt}{Nb}\theta'' = 0. \tag{31}$$

The associated boundary conditions become

$$f(0) = 0,\ F(0) = \lambda,\ g(0) = 0,\ G'(0) = 0,$$
$$\theta(0) = 1,\ \varphi(0) = 1, \tag{32a}$$

$$F(\infty) = 1,\ G(\infty) = 1,\ \theta(\infty) = 0,\ \varphi(\infty) = 0. \tag{32b}$$

In the context of the SRM algorithm, we obtain the following iteration scheme:

$$F''_{r+1} + f_r\,F'_{r+1} = \beta g_r G'_r, \tag{33}$$

$$f'_{r+1} = F_{r+1}, \tag{34}$$

$$\frac{1}{Prm}G''_{r+1} + f_{r+1}G'_{r+1} - g_r\,G'_{r+1} = 0, \tag{35}$$

$$g'_{r+1} = G_{r+1}, \tag{36}$$

$$\frac{1+Rd}{Pr}\theta''_{r+1} + f_{r+1}\theta'_{r+1} + Nb\theta'_{r+1}\varphi'_r = -Nt\theta'^2_r, \tag{37}$$

$$\varphi''_{r+1} + Lef_{r+1}\,\varphi'_{r+1} = -\frac{Nt}{Nb}\theta''_{r+1}. \tag{38}$$

Subject to the boundary conditions:

$$F_{r+1}(0) = \lambda, F_{r+1}(\infty) = 1, \tag{39}$$

$$f_{r+1}(0) = 0, \tag{40}$$

$$G'_{r+1}(0) = 0, G'_{r+1}(\infty) = 1, \tag{41}$$

$$g_{r+1}(0) = 0, \tag{42}$$

$$\theta_{r+1}(0) = 1, \theta_{r+1}(\infty) = 0, \tag{43}$$

$$\varphi_{r+1}(0) = 1, \varphi_{r+1}(\infty) = 0. \tag{44}$$

To solve equations (33)–(38), we discretize them using the Chebyshev spectral method. For brevity, we omit the details of the Spectral method and refer interested readers to the standard monographs of Canuto *et al.* (1988) and Trefethen (2000). To apply the spectral method, the domain is transformed to the interval $[-1, 1]$ on which the governing equation is defined. The transformation $\eta = L(\tau + 1)/2$ is used to map the interval $[0, L]$ to $[-1, 1]$, where L is chosen to be large enough to approximate the conditions at infinity numerically. In spectral collocation methods, a differentiation matrix $\mathbf{D}$ of size $(N + 1) \times (N + 1)$ is introduced,

Downloaded from https://academic.oup.com/jcde/article/8/4/1158/6324282 by University of Salford user on 29 July 2021

which is used to approximate the derivatives of the unknown variables at the collocation points as the matrix vector

$$\frac{df_r}{d\eta} = \sum_{k=0}^{N} D_{jk} f_r(\tau_k) = \mathbf{D}\mathbf{f}_r, \quad j = 1, 2, \ldots\ldots\ldots\ldots N, \tag{45}$$

where $(N + 1)$ is the number of collocation points (grid points), $\mathbf{D} = \frac{2D}{L}$, and $\mathbf{f} = [f(\tau_0), f(\tau_1), \ldots\ldots\ldots, f(\tau_N)]^T$ is the vector function at the collocation points. Higher order derivatives are obtained as powers of $\mathbf{D}$, i.e.

$$f_r^{(p)} = \mathbf{D}^p \mathbf{f}_r, \tag{46}$$

where p is the order of derivatives. We choose the Gauss–Lobatto collocation points to define the nodes in $[-1, 1]$ as follows:

$$\tau_j = \cos\left(\frac{\pi j}{N}\right), \quad j = 0, 1, 2, \ldots.., N. \tag{47}$$

Applying the Chebyshev pseudo-spectral method on equations (33) to (38), we obtain

$$A_1\mathbf{F}_{r+1} = R_1, \quad F_{r+1}(\tau_{\tilde{N}}) = \lambda, \; F_{r+1}(\tau_0) = 1, \tag{48}$$

$$A_2\mathbf{f}_{r+1} = R_2, \quad f_{r+1}(\tau_{\tilde{N}}) = 0, \tag{49}$$

$$A_3\mathbf{G}_{r+1} = R_3, \quad G'_{r+1}(\tau_{\tilde{N}}) = 0, \; G_{r+1}(\tau_0) = 1, \tag{50}$$

$$A_4\mathbf{g}_{r+1} = R_4, \quad g_{r+1}(\tau_{\tilde{N}}) = 0, \tag{51}$$

$$A_5\boldsymbol{\theta}_{r+1} = R_5, \quad \theta_{r+1}(\tau_{\tilde{N}}) = 0, \; \theta_{r+1}(\tau_0) = 1, \tag{52}$$

$$A_6\boldsymbol{\varphi}_{r+1} = R_6, \quad \varphi_{r+1}(\tau_{\tilde{N}}) = 0, \; \varphi_{r+1}(\tau_0) = 1. \tag{53}$$

Here,

$$A_1 = \mathbf{D}^2 + \mathrm{diag}[\mathbf{f}_r]\mathbf{D}, \quad R_1 = \beta\mathbf{g}_r\mathbf{G}'_r, \tag{54}$$

$$A_2 = \mathbf{D}, \quad R_2 = \mathbf{F}_{r+1}, \tag{55}$$

$$A_3 = \frac{1}{Prm}\mathbf{D}^2 + \mathrm{diag}[\mathbf{f}_{r+1} - \mathbf{g}_r]\mathbf{D}, \quad R_3 = \mathbf{O}, \tag{56}$$

$$A_4 = \mathbf{D}, \quad R_4 = \mathbf{G}_{r+1}, \tag{57}$$

$$A_5 = \left(\frac{1 + Rd}{Pr}\right)\mathbf{D}^2 + \mathrm{diag}[\mathbf{f}_{r+1} + Nb]\mathbf{D}, \quad R_5 = -Nt\boldsymbol{\theta}'^2_r, \tag{58}$$

$$A_6 = \mathbf{D}^2 + \mathrm{diag}[Le\mathbf{f}_{r+1}]\mathbf{D}, \quad R_6 = -\frac{Nt}{Nb}\boldsymbol{\theta}''_r. \tag{59}$$

In equations (39)–(44), the size of the matrix $\mathbf{O}$ is $(\tilde{N} + 1) \times 1$, diag [] is a diagonal matrix, all of size $(\tilde{N} + 1) \times (\tilde{N} + 1)$, where $\tilde{N}$ is the number of grid points, $\mathbf{f}$, $\mathbf{g}$, $\mathbf{F}$, $\mathbf{G}$, $\boldsymbol{\theta}$, and $\boldsymbol{\varphi}$ are the values of f, g, F, G, θ, and φ, respectively, when evaluated at the grid points, and the subscript r denotes the iteration number. Equations (39)–(44) constitute the SRM scheme and can be solved using the spectral collocation method starting from the following initial conditions, which are chosen to satisfy the boundary conditions:

$$f_0(\eta) = \eta + (\lambda - 1)(1 - e^{-\eta}), \quad F_0(\eta) = 1 + (\lambda - 1)e^{-\eta},$$
$$G_0(\eta) = 1, \quad g_0(\eta) = \eta, \quad \theta_0(\eta) = e^{-\eta}, \quad \varphi_0(\eta) = e^{-\eta}. \tag{60}$$

CPU times are of the order of several minutes, and the solutions converge quickly.

5. Validation of SRM

The nonlinear boundary value problem is defined by equations (12)–(15) subject to the boundary conditions (16a) to (16b) have been solved numerically using the SRM. The numerical method is programmed using the MATLAB R2018a software. The SRM results are obtained here using $N = 50$ collocation points, and the infinity value η_∞ is taken as 15. In this study, the following default parameter values are adopted for computations: Pr = 0.7, Prm = 0.5, $\lambda = 0.1$, $\beta = 0.1$, Nt = 0.1, Nb = 0.3, Rd = 0.5, and Le = 5. These data correspond to metallic nanofluids in base fluids, which reduces the Prandtl number, have strong magnetic induction, appreciable radiative flux, and species diffusivity twice the thermal diffusivity (Le = 0.5), and follow references Daniel *et al.* (2018) (for radiative effect), Das *et al.* (2007), Bég *et al.* (2014), Uddin *et al.* (2015), and Aly and Sayed (2017) (for nanofluids), and Hughes and Young (1966) (for electromagnetic drag and induction effects). All data are realistic and apply to the case studied, i.e. magnetic nanofluid stretching sheet flow for coating. All graphs therefore conform to these values unless stated explicitly otherwise. To verify the accuracy of the SRM, the results are compared with the earlier solutions of Shateyi and Prakash (2014) and shown in Table 1 for skin friction, $-f''(0)$ with different values of sheet velocity parameter, λ. Excellent agreement is achieved testifying the accuracy of the present SRM code.

Table 1: Comparison of SRM solutions for $-f''(0)$.

Λ	SRM	Shateyi and Prakash (2014)
0.1	0.46251223	0.46251223
0.2	0.44315478	0.44315478
0.4	0.37509516	0.37509516
0.5	0.32874112	0.32874112

6. Results and Discussion

Extensive computations have been conducted in MATLAB, and SRM solutions are shown in Tables 2–4 and Figs 2–18.

Table 2 represents the effects of Prandtl number Pr, radiation parameter Rd, moving surface (sheet velocity) parameter λ, Brownian motion parameter Nb and thermophoresis parameter Nt on the skin-friction coefficient C_f, the reduced Nusselt number Nu, and the reduced Sherwood number Sh. It is observed that the rate of heat transfers at the surface increases with more significant Prandtl number (lower thermal conductivity of magnetic nanofluid reduces temperatures in the boundary layer and encourages heat transfer to the wall). In contrast, the rate of mass transfer is diminished as the Prandtl number increases (nanoparticle concentration is increased in the boundary layer regime, which decreases the rate of nanoparticle mass transfer to the wall). Increasing the Lewis number Le, and the radiation parameter Rd, increases the reduced Sherwood number at the border (more significant Lewis number implies higher thermal diffusivity relative to nanoparticle mass diffusivity, which boosts nanoparticle concentrations in the fluid regime and suppresses transport to the wall). In contrast, it reduces the heat transfer rate at the border (higher radiative flux elevates temperatures in the boundary layer, which diminishes the transfer of heat to the wall). It is also evident that increasing moving surface parameter value λ decreases the skin friction at the wall plate (since this serves to inhibit boundary layer growth and destroys momentum leading to deceleration), whereas it manifests in an elevation in reduced Nusselt and Sherwood numbers, i.e. significantly enhancing heat and nanoparticle diffusion to the wall. An increase in the Brownian motion parameter

Downloaded from https://academic.oup.com/jcde/article/8/4/1158/6324282 by University of Salford user on 29 July 2021

Table 2: Skin-friction coefficient C_f, the reduced Nusselt number Nu, and the reduced Sherwood number Sh with Prm = 0.71, β = 0.1.

Pr	Le	Rd	λ	Nb	Nt	$f''(0)$	$-\theta'(0)$	$-\phi'(0)$
1	2	1	0.1	0.1	0.1	0.43850546	0.24324811	0.62176714
2	2	1	0.1	0.1	0.1	0.43850546	0.32268809	0.59315154
1	10	1	0.1	0.1	0.1	0.43850546	0.24543873	1.20585872
1	2	2	0.1	0.1	0.1	0.43850546	0.20192103	0.63398262
1	2	1	0.5	0.1	0.1	0.30817145	0.27678430	0.84214287
1	2	1	0.1	0.5	0.1	0.43850546	0.27990286	0.64700386
1	2	1	0.1	0.1	0.5	0.43850546	0.23536033	0.49264088

Table 3: Reduced Nusselt number Nu with Prm = 0.71, β = 0.1, Le = 1, Nb = Nt = 0.3, Rd = 1.

Λ	$-\theta'(0)$, Pr = 0.71	$-\theta'(0)$, Pr = 5	$-\theta'(0)$, Pr = 10
−0.3	0.17039064	0.27824451	0.30238506
0.1	0.22008309	0.46040570	0.54910057
0.5	0.24559296	0.56481218	0.69755154
1	0.26900089	0.66560004	0.84272786
1.5	0.28787633	0.74959618	0.96437941
2	0.30409146	0.82329138	1.07133585

Table 4: Reduced Sherwood number Sh with Pr = 0.71, Prm = 0.71, β = 0.1, Nb = Nt = 0.3, Rd = 1.

Λ	$-\phi'(0)$, Le = 1	$-\phi'(0)$, Le = 5	$-\phi'(0)$, Le = 10
−0.3	0.23757681	0.21076314	0.12930055
0.1	0.46154611	0.90775090	1.20149742
0.5	0.59332949	1.33118606	1.86506212
1	0.72134948	1.73296536	2.47937544
1.5	0.82831705	2.06229602	2.97641263
2	0.92225761	2.34770012	3.40422563

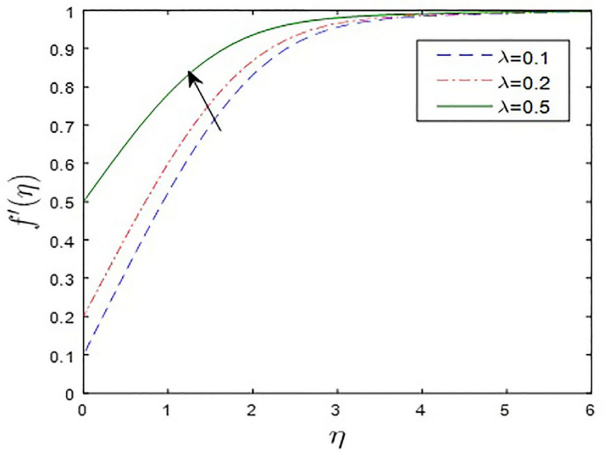

Figure 2: Velocity profiles for different values of sheet velocity parameter, λ.

Nb and thermophoresis parameter Nt has no substantial influence on the skin-friction coefficient. The rate of heat and mass transfer at the wall, however, increases as the Brownian motion parameter increases (which corresponds to smaller nanoparticles and encourages thermal and species diffusion to the boundary). Both the Nusselt number and the Sherwood number are reduced as the values of the thermophoresis parameter increase

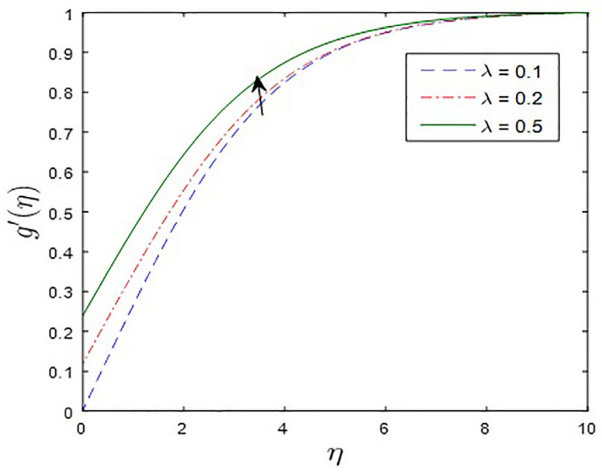

Figure 3: Induced magnetic stream function gradient for different sheet velocity parameters, λ.

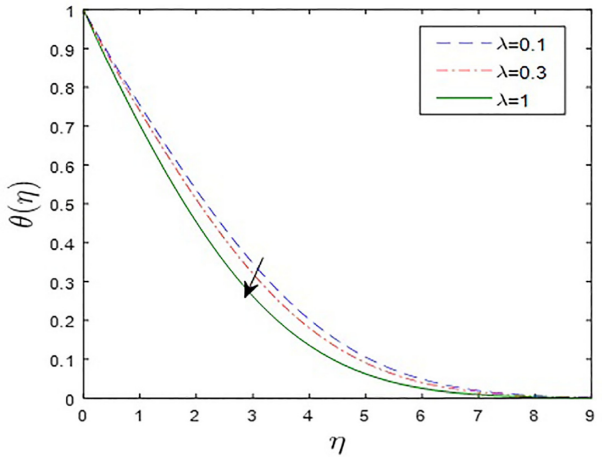

Figure 4: Temperature profiles for different values of sheet velocity parameter, λ.

since temperatures and nanoparticle concentration magnitudes in the boundary layer are elevated, and this mitigates transfer to the wall, as noted by many other researchers, e.g. Hamad *et al.* (2011) and Haddad *et al.* (2012).

Table 3 depicts the heat transfer rate for various values of Prandtl number Pr with other flow parameters constrained. With negative wall velocity, the reduced Nusselt number is reduced, whereas with positive wall velocity, it is consistently elevated at all Prandtl number values.

Downloaded from https://academic.oup.com/jcde/article/8/4/1158/6324282 by University of Salford user on 29 July 2021

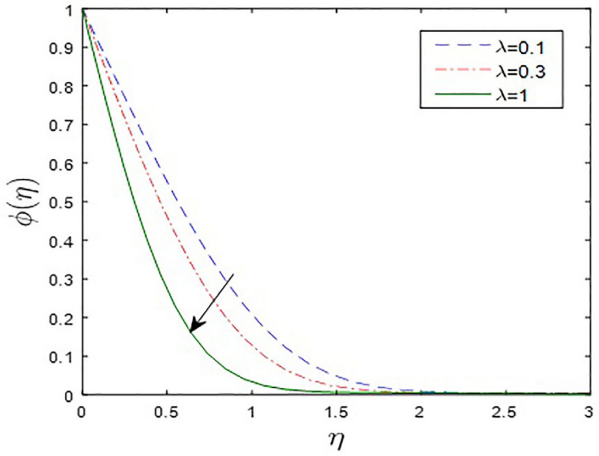

Figure 5: Nanoparticle concentration profiles for different values of sheet velocity parameter, λ.

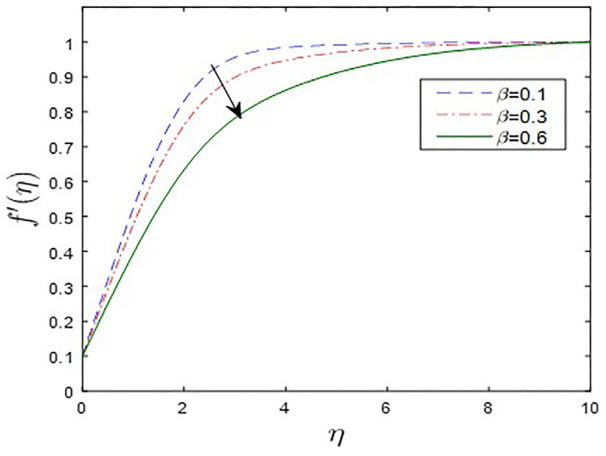

Figure 6: Velocity profiles for different values of magnetic force parameter, β.

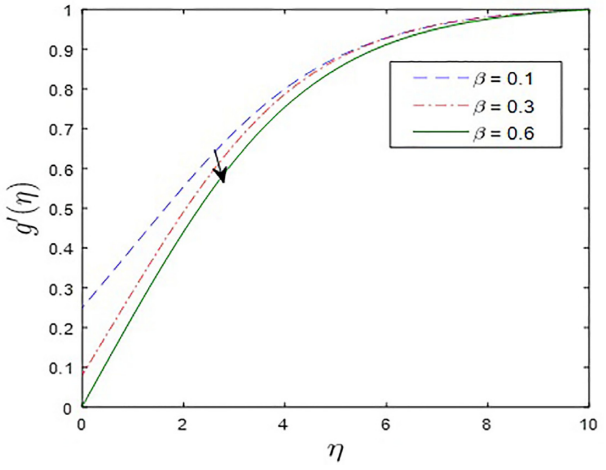

Figure 7: Induced magnetic stream function gradient for various magnetic force parameters, β.

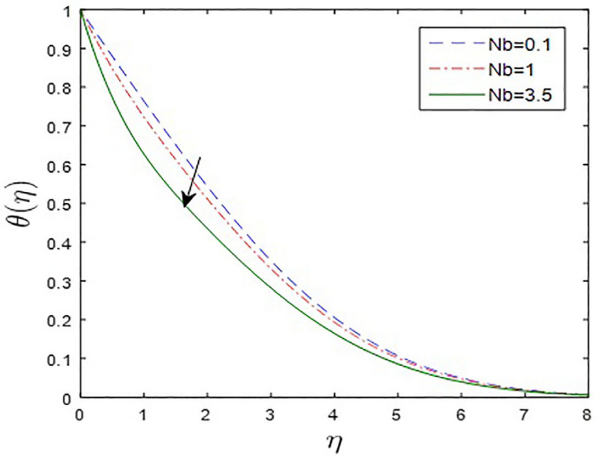

Figure 8: Temperature profiles for different values of Brownian motion parameter, Nb.

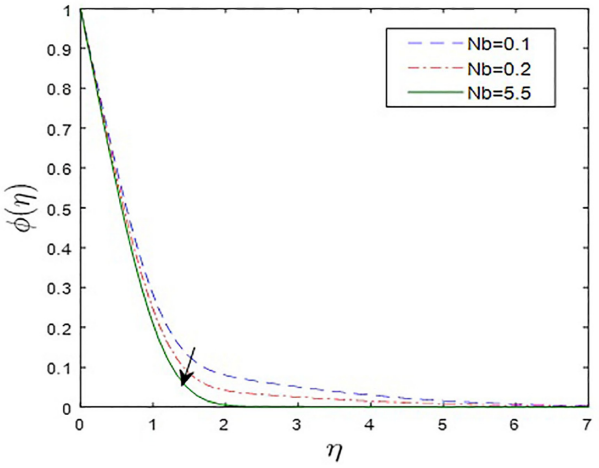

Figure 9: Nanoparticle concentrations for different values of Brownian motion parameter, Nb.

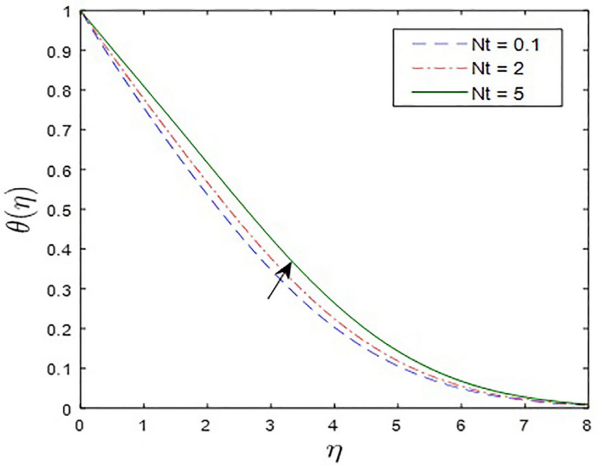

Figure 10: Temperature profiles for different values of thermophoresis parameter, Nt.

Downloaded from https://academic.oup.com/jcde/article/8/4/1158/6324282 by University of Salford user on 29 July 2021

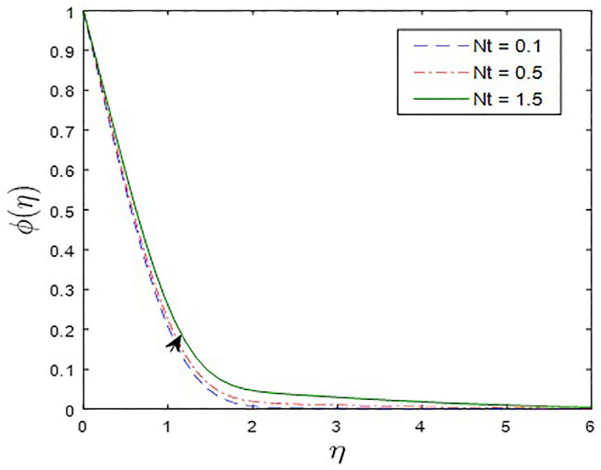

Figure 11: Nanoparticle concentration profiles for different thermophoresis parameters, Nt.

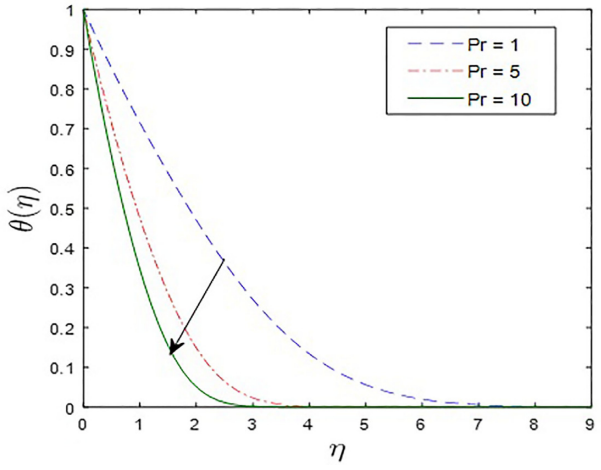

Figure 12: Temperature profiles for different values of Prandtl number, Pr.

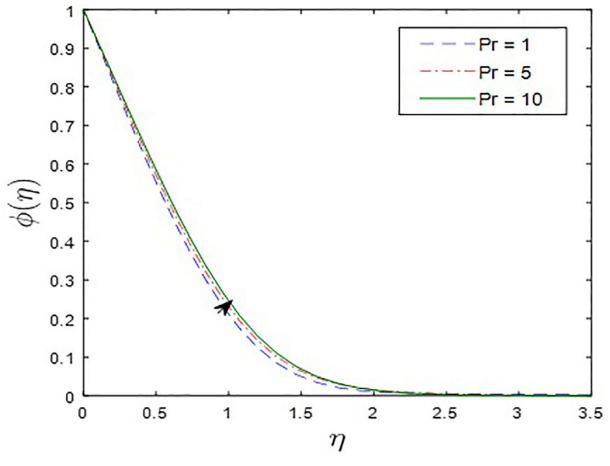

Figure 13: Nanoparticle concentration profiles for different values of Prandtl number, Pr.

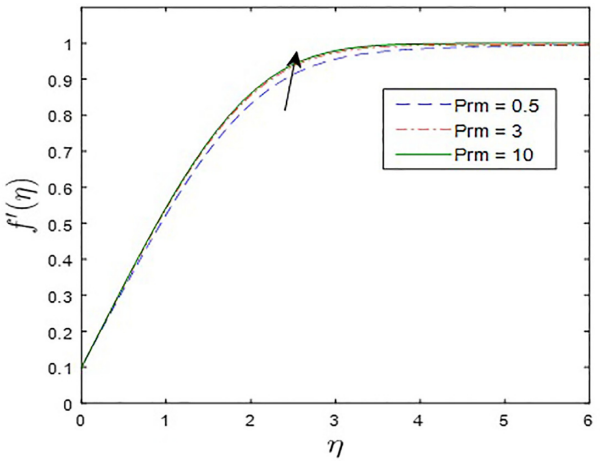

Figure 14: Velocity profiles for different values of magnetic Prandtl number, Prm.

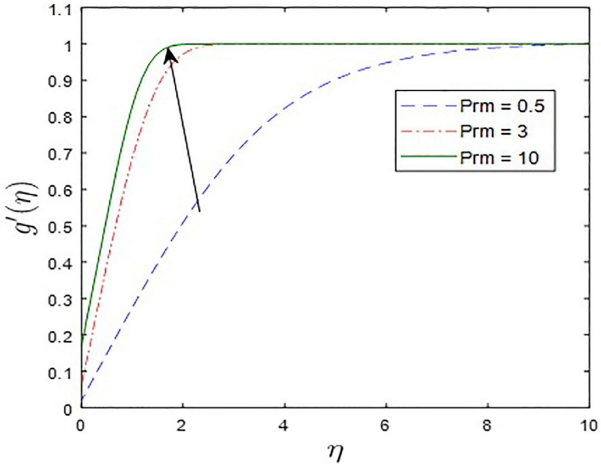

Figure 15: Induced magnetic stream function gradient for different magnetic Prandtl numbers, Prm.

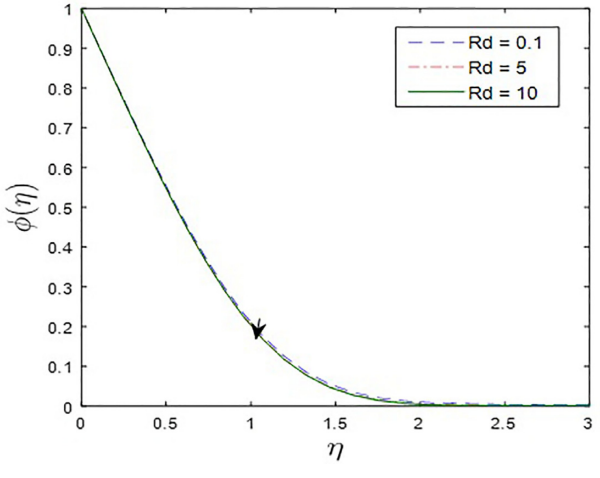

Figure 16: Nanoparticle concentration profiles for different values of radiation parameter, Rd.

Downloaded from https://academic.oup.com/jcde/article/8/4/1158/6324282 by University of Salford user on 29 July 2021

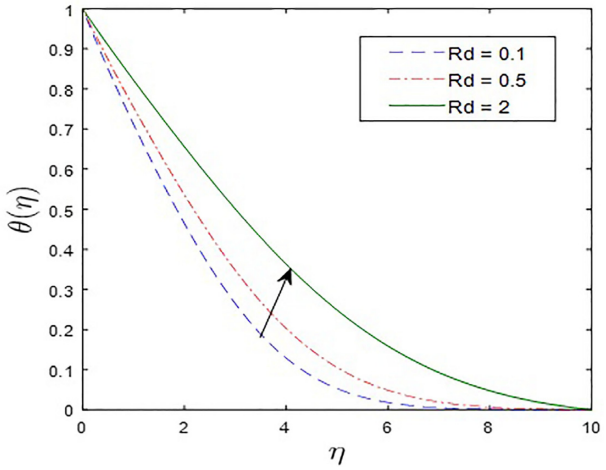

Figure 17: Temperature profiles for different values of radiation parameter, Rd.

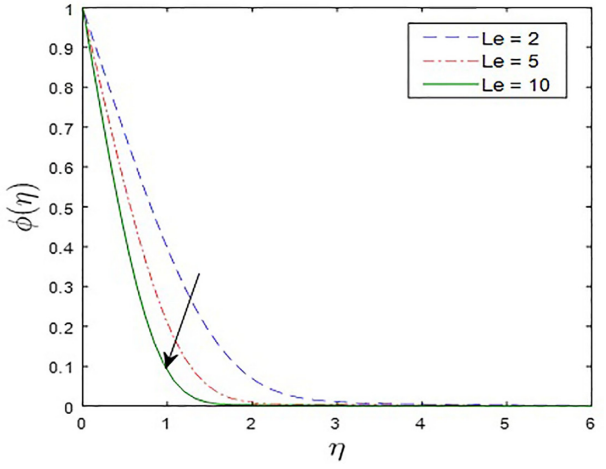

Figure 18: Nanoparticle concentration profiles for different values of Lewis number, Le.

Table 4 depicts the mass transfer rate (reduced Sherwood number) for different Lewis number Le values with other parameters constant. Reduced Sherwood number is lowered with increasing Lewis number, for negative wall velocity, whereas it is enormously increased with more significate Lewis number for the positive wall velocity case.

Table 5 demonstrates the influence of various magnetic force parameters, β, with different sheet velocity parameters, λ, on skin-friction coefficient C_f. It is noticed that the skin-friction coefficient reduced very rapidly due to increase in the values of these parameters.

Figures 2–5 display the effects of moving wall velocity parameter, λ, on velocity, induced magnetic field, temperature, and nanoparticle concentration profiles. It is seen that increasing the velocity parameter λ leads to an increase of speed (Fig. 2), i.e. flow acceleration and induced magnetic field (Fig. 3) magnitudes. Hydrodynamic boundary layer thickness is therefore decreased, whereas magnetic boundary layer thickness is enhanced. Asymptotically smooth profiles are achieved in the free stream, verifying that an adequately large infinity boundary condition is prescribed in the MATLAB SRM code. Temperature (Fig. 4) and nanoparticle concentration (Fig. 5) are both

Table 5: Skin-friction coefficient C_f with Pr = 0.7, Prm = 0.5, λ = 0.1, Nt = 0.1, Nb = 0.3, Rd = 0.5 , and Le = 5.

λ	$-f''(0)$ β = 0.1	$-f''(0)$ β = 0.2	$-f''(0)$ β = 0.3
0.1	0.46187385	0.46119457	0.46049300
0.2	0.44273586	0.44229701	0.44184741
0.3	0.41319222	0.41280996	0.41241846
0.4	0.37464177	0.37417205	0.37368768
0.5	0.32805632	0.32734220	0.32659778
0.6	0.27411112	0.27291390	0.00069248
0.7	0.21317965	0.21099046	0.00085186
0.8	0.14491586	0.00168838	0.00099312
0.9	0.00321266	0.00167927	0.00098807

strongly decreased with increasing moving wall velocity parameters. Thermal boundary layer and nanoparticle concentration boundary layer thickness are both therefore suppressed with larger velocity of the moving wall, λ.

Figures 6 and 7 visualize the effects of magnetic force number, β, on the velocity and induced magnetic field profiles. This parameter features in the magnetic induction term in the dimensionless momentum boundary layer equation (9), $-\beta gg''$, which also couples the momentum equation (9) to the magnetic induction equation (10). It is an opposing body force, and increasing values of β will therefore inhibit momentum and magnetic induction in the regime. This will manifest as a decrease in velocity and induced magnetic field magnitudes and a concomitant elevation in momentum boundary layer thickness and depletion in magnetic boundary layer thickness, as noted earlier by Hughes and Young (1966), among other researchers.

Figures 8 and 9 depict the influence of Brownian motion parameter Nb on temperature and nanoparticle concentration profiles. Temperature and nanoparticle concentration noticeably decrease with the increase of Nb. Conversely, in Figs 10 and 11, increasing thermophoresis parameter Nt significantly elevates temperature and concentration profiles. Thermophoretic body force encourages heat and nanoparticle mass diffusion with thermal gradient. Thermal boundary layer and nanoparticle concentration boundary layer thickness are therefore both accentuated with greater thermophoretic body force. These trends concur with many other investigations, including Bachok *et al.* (2010), Ferdows *et al.* (2012), and Mabood *et al.* (2015), although these studies neglected magnetic induction effects. The nanoscale effects, i.e. Brownian motion and thermophoresis, do not exert any significant influence on either nanofluid velocity or induced magnetic field profile, and therefore, these graphs are omitted for brevity.

Figures 12 and 13 illustrate the variation of temperature and nanoparticle concentration distributions in response to a change in Prandtl number Pr. Increasing the Prandtl number Pr induces a substantial decrease in nanofluid temperature and suppresses thermal boundary layer thickness. The nanoparticle concentration profiles exhibit a monotonic response to Prandtl number, i.e. as Pr increases, nanoparticle diffusion is encouraged, and the nanoparticle concentration boundary layer thickness is also increasing.

Figures 14 and 15 visualize the impact of magnetic Prandtl number Prm on the velocity and induced magnetic field profiles. Both velocity and induced magnetic field profiles of the nanofluid increase with elevation in Prm. This parameter equals $\frac{\nu}{\alpha_1}$ and is invoked because of magnetic induction effects and determines the ratio of magnetic diffusivity to viscous diffusivity. It

Downloaded from https://academic.oup.com/jcde/article/8/4/1158/6324282 by University of Salford user on 29 July 2021

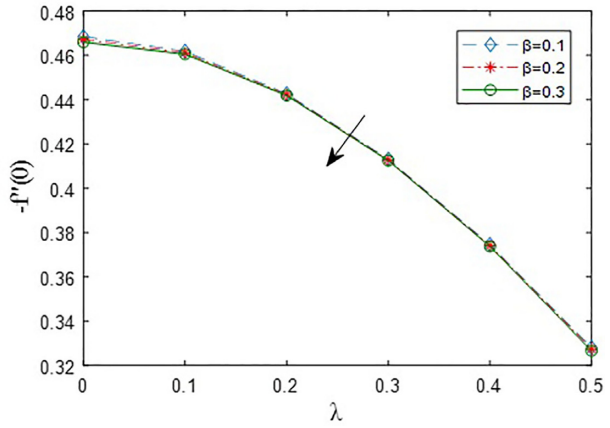

Figure 19: Influences of magnetic force parameter, β, and sheet velocity parameter, λ, on skin-friction coefficient C_f.

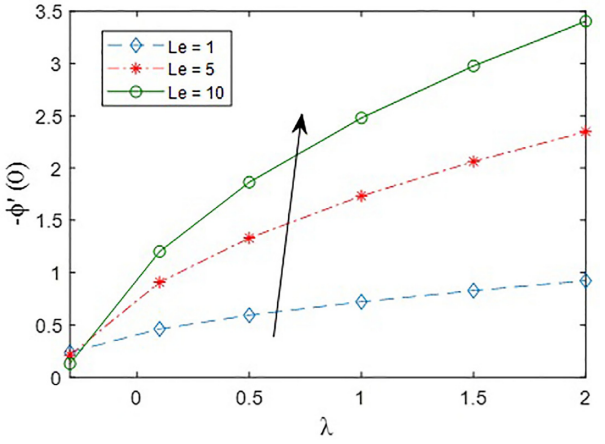

Figure 21: Influences of Lewis number, Le, and sheet velocity parameter, λ, on Reduced Sherwood number Sh.

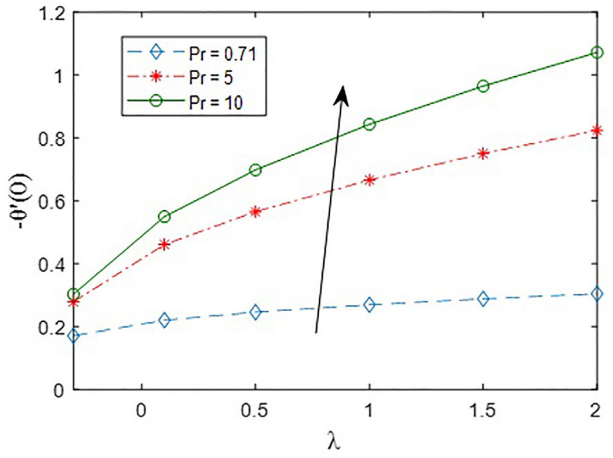

Figure 20: Influences of Prandtl number, Pr, and sheet velocity parameter, λ, on Reduced Nusselt number Nu.

features exclusively magnetic induction conservation equation (10). Thus, the magnetic Reynolds number is high enough for the flow field to cause magnetic field distortion. The magnetic field is considered to be undistorted by the flow for a case where this parameter is very weak (as compared with unity). However, the induction effects of large values of magnetic Reynolds number are significant and necessitate a separate conservation equation, as considered in the present model. As Prm is elevated, both momentum and magnetic induction are assisted in the regime. Momentum and magnetic boundary layer thicknesses will therefore be, respectively, increased and decreased. It is also apparent that the effect of Prm is more pronounced on magnetic induction $g'(\eta)$ compared to $f'(\eta)$.

Figures 16 and 17 depict the influence of the radiation parameter Rd on nanoparticle volume fraction (concentration) and the temperature distribution, respectively, occuring in the augmented thermal diffusion term in the energy conservation equation (11), viz. $(\frac{1+Rd}{Pr})\theta''$. $Rd = \frac{16\sigma^* T_\infty^3}{3KK_s}$ and expresses the relative contribution of thermal radiation heat transfer to thermal conduction heat transfer. When $Rd = 1$, both modes contribute equally. For $Rd < 1$, conduction dominates and vice versa for $Rd > 1$. An increase in Rd leads to a decrease of the nanoparticle volume fraction (Fig. 16) since *greater energization of the nanofluid with radiative flux inhibits nanoparticle diffusion*; however, the converse response is induced on temperature magnitudes (Fig. 17) that are strongly elevated with a greater radiative contribution. Nanoparticle concentration boundary layer thickness is therefore decreased, whereas thermal boundary layer thickness is enhanced with greater radiative parameter (which concurs with the earlier decrease in reduced Nusselt number at the wall). The computations agree with several other investigations, including Aly and Sayed (2017) and Uddin *et al.* (2015). The inclusion of radiative heat transfer in magnetic nanomaterials fabrication therefore produces more accurate temperature and nanoparticle concentration predictions than neglecting this mode of heat transfer (which leads to underprediction in temperatures and overprediction in nanoparticle volume fractions).

Finally, Fig. 18 illustrates the variation of nanoparticle concentration profile with the Lewis number Le. $Le = \frac{\nu}{D_B}$ and defines the ratio of momentum diffusion rate to nanoparticle species diffusion rate. When $Le = 1$, these rates are equal, and both momentum and nanoparticle concentration boundary layer thicknesses are similar. However, for $Le > 1$ (as considered here), momentum diffusivity exceeds species diffusivity of the nanoparticles, which inhibits nanoparticle diffusion and results in a depletion in nanoparticle concentration boundary layer thickness. The latter may therefore be successfully controlled in nanoliquid material processing via careful selection of nanoparticles based on appropriate diffusivities.

Figures 19–21 demonstrate the graphs of the skin-friction coefficient C_f, the reduced Nusselt number Nu, and the reduced Sherwood number Sh for different values of magnetic parameter, Prandtl number, and Lewis number, respectively, with velocity parameter. The values of the skin-friction coefficient C_f decrease as the magnetic force parameter enhances and with the increasing values of the Prandtl number, the reduced Nusselt number Nu increases very rapidly. The reduced Sherwood number Sh gets enhanced due to increase in the values of Lewis number.

7. Conclusions

A mathematical study has been presented for steady 2D MHD thermal convection boundary layer flow of electroconductive nanofluids over a moving surface in a uniform free stream with magnetic induction and radiative heat transfer effects. The

Downloaded from https://academic.oup.com/jcde/article/8/4/1158/6324282 by University of Salford user on 29 July 2021

Buongiorno model has been deployed, which incorporates the results of Brownian diffusion and thermophoresis. The partial differential equations governing the flow and heat transfer were transformed into coupled nonlinear ordinary differential equations using appropriate similarity transformations. The resulting equations were then solved by an accurate iterative method known as the SRM. The SRM algorithm is straightforward to implement since it can be constructed directly from the governing equations in their original form. Validation of the MATLAB SRM code with published results is included. The variations of the skin-friction coefficient, the heat transfer rate, and the mass transfer rate, as well as the velocity, induced magnetic field, temperature, and the nanoparticle volume fraction profiles, are illustrated in tabular and graphical forms for various values of the physical parameters. From this study, some fundamental results are summarized as follows:

1. Velocity and induced magnetic field profiles decrease with an increase in magnetic body force parameters.
2. Thermal boundary layer thickness is enhanced with increasing magnetic body force parameter, thermophoresis parameter, and radiative parameter. In contrast, they are diminished with more incredible wall velocity, Brownian motion, and Prandtl numbers.
3. The induced magnetic field stream function is affected the most by reciprocating the magnetic Prandtl number Pr_m compared with the skin-friction and heat transfer coefficients.
4. Nanoparticle concentration improves with higher values of thermophoresis and Prandtl number, whereas it is suppressed with increasing moving wall, Brownian motion, radiative, and Lewis numbers.

This study has shown that SRM is a versatile and powerful numerical technique for nonlinear electromagnetic induction nanofluid materials processing flows. However, attention has been confined to Newtonian nanofluids. Future studies will explore rheological nanofluid behavior, including viscoelastic (Rana *et al.*, 2017) and viscoplastic (Thumma *et al.*, 2020) models, and will be communicated imminently. This study may be generalized also to consider electrical field effects (Bég *et al.*, 2013), and this is also presently under consideration. Additionally, several other physicochemical products arise in magnetic nanomaterial synthesis, including geometrical shape effects of nanoparticles (Saleem *et al.*, 2020), Hiemenz stagnation and slip flows (Nadeem *et al.*, 2020), Hall current effects (Bhatti *et al.*, 2019), and bioconvection effects in which nanoparticles are combined with micro-organism doping to achieve dual benefits (Bhatti *et al.*, 2020). Furthermore, alternative nanoparticles, e.g. molybdenum disulfide (Sowmya *et al.*, 2019) and triple diffusion (Archana *et al.*, 2018) (double nanoparticle species), may also be considered, and efforts in this direction are also being explored. All these areas constitute interesting directions for the refinement of the present simulations with the SRM numerical approach.

Funding

This research did not receive any specific grant from funding agencies in the public, commercial, or not-for-profit sectors.

Conflict of interest statement

None declared.

References

Abu-Nada, E. (2008). Application of nanofluids for heat transfer enhancement of separated flows encountered in a backward facing step. *International Journal of Heat and Fluid Flow*, 29, 242–249.

Ali, N., Teixeira, J. A., & Addali, A. (2018). A review on nanofluids: Fabrication, stability, and thermophysical properties. *Journal of Nanomaterials*, *2018*, 6978130. https://doi.org/10.1155/2018/6978130.

Aly, E. H., & Sayed, H. M. (2017). Magnetohydrodynamic and thermal radiation effects on the boundary-layer flow due to a moving extensible surface with the velocity slip model: A comparative study of four nanofluids. *Journal of Magnetism and Magnetic Materials*, *42215*, 440–451.

Archana, M., Reddy, M. G., Gireesha, B. J., Prasannakumara, B. C., & Shehzad, S. A. (2018). Triple diffusive flow of nanofluid with buoyancy forces and nonlinear thermal radiation over a horizontal plate. *Heat Transfer*, *47*(8), 957–973.

Awad, F. G., Motsa, S., & Khumalo, M. (2014). Heat and mass transfer in unsteady rotating fluid flow with binary chemical reaction and activation energy. *Plos One*, 9(9), e107622.

Bachok, N., Ishak, A., & Pop, I. (2010). Boundary layer flow of nanofluids over a moving surface in a flowing fluid. *International Journal of Thermal Sciences*, 49, 1663–1668.

Bég, O. A. (2018). Nonlinear multi-physical laminar nanofluid bioconvection flows: Models and computation. In A. Sohail, & Z. Li (Eds.), *Computational approaches in biomedical nanoengineering*(Chapter 5, pp. 113–145). Wiley.

Bég, O. A., Ferdows, M., Islam, S., & Nazrul Islam, M. (2014). Numerical simulation of Marangoni magnetohydrodynamic bio-nanofluid convection from a non-isothermal surface with magnetic induction effects: A bio-nanomaterial manufacturing transport model. *Journal of Mechanics in Medicine and Biology*, *14*(3), 1450039.1–1450039.32.

Bég, O. A., Hameed, M., & Bég, T. A. (2013). Chebyschev spectral collocation simulation of nonlinear boundary value problems in electrohydrodynamics. *International Journal of Computational Methods in Engineering Science and Mechanics*, *14*, 104–115.

Bég, O. A., Khan, M. S., Karim, I., Alam, M. M., & Ferdows, M. (2014). Explicit numerical study of unsteady hydromagnetic mixed convective nanofluid flow from an exponentially stretching sheet in porous media. *Applied Nanoscience*, *4*(8), 943–957.

Bég, O. A., Motsa, S. S., Islam, M. N., & Lockwood, M. (2014). Pseudo-spectral and variational iteration simulation of exothermically-reacting Rivlin-Ericksen viscoelastic flow and heat transfer in a rocket propulsion duct. *Computational Thermal Sciences*, *6*(2), 91–102.

Bég, O. A., Motsa, S. S., Kadir, A., Bég, T. A., & Islam, M. N. (2016). Spectral quasilinear numerical simulation of micropolar convective wall plumes in high permeability porous media. *Journal of Engineering Thermophysics*, *25*(4), 1–24.

Bhatti, M. M., Ellahi, R., Zeeshan, A., Marin, M., & Ijaz, N. (2019). Numerical study of heat transfer and Hall current impact on peristaltic propulsion of particle-fluid suspension with compliant wall properties. *Modern Physics Letters B*, *33*(35), 1950439.

Bhatti, M. M., Shahid, A., Abbas, T., Alamri, S. Z., & Ellahi, R. (2020). Study of activation energy on the movement of gyrotactic microorganism in a magnetized nanofluids past a porous plate. *Processes*, *8*(3), 328.

Buongiorno, J. (2006). Convective transport in nanofluids. *ASME Journal of Heat Transfer*, *128*(3), 240–250.

Downloaded from https://academic.oup.com/jcde/article/8/4/1158/6324282 by University of Salford user on 29 July 2021

Canuto, C., Hussaini, M. V., Quarteroni, A., & Zang, T. A. (1988). *Spectral methods in fluid dynamics*. Springer.

Chamakha, A. J. (1997). Hydromagnetic natural convection from an isothermal inclined surface adjacent to a thermally stratified porous medium. *International Journal of Engineering Science*, *35*, 975–986.

Chamkha, A. J. (1997). Solar radiation assisted convection in uniform porous medium supported by a vertical plate. *ASME Journal of Heat Transfer*, *119*, 89–96.

Choi, S. U. S. (1995). Enhancing thermal conductivity of fluids with nanoparticles. In *The Proceedings of ASME International Mechanical Engineering Congress and Exposition*(pp. 99–105).

Choi, S. U. S. (2009). Nanofluids: From vision to reality through research. *ASME Journal of Heat Transfer*, *131*(3), 1–9.

Choi, S. U. S., Zhang, Z. G., & Keblinski, P. (2004). Nanofluids. In H. S. Nalwa (Ed.), *Encyclopedia of nanoscience and nanotechnology*(Vol. *6*, pp. 757–737). American Scientific.

Choi, S. U. S., Zhang, Z. G., Yu, W., Lockwood, F. E., & Grulke, E. A. (2001). Anomalous thermal conductivity enhancement in nanotube suspensions. *Applied Physics Letters*, *79*(14), 2252–2254.

Daniel, Y. S., Aziz, Z. A., Ismail, Z., & Salah, F. (2018). Thermal stratification effects on MHD radiative flow of nanofluid over nonlinear stretching sheet with variable thickness. *Journal of Computational Design and Engineering*, *5*(2), 232–242.

Das, S. K., Choi, S. U. S., & Patel, H. E. (2006). Heat transfer in nanofluids - A review. *Heat Transfer Engineering*, *27*(10), 3–19.

Das, S. K., Choi, S. U. S., Yu, W., & Pradeep, T. (2007). *Nanofluids: Science and technology*. Wiley.

Das, K., Sharmab, R. P., & Sarkar, A. (2016). Heat and mass transfer of a second grade magnetohydrodynamic fluid over a convectively heated stretching sheet. *Journal of Computational Design and Engineering*, *3*(4), 330–336.

Ferdows, M., Khan, M. S., Alam, M. M., & Sun, S. (2012). MHD mixed convective boundary layer flow of a nanofluid through a porous medium due to an exponentially stretching sheet. *Mathematical Problems in Engineering*, *2012*, 408528.

Ferdows, M., Khan, M. S., Bég, O. A., Azad, M. A. K., & Alam, M. M. (2014). Numerical study of transient magnetohydrodynamic radiative free convection nanofluid flow from a stretching permeable surface. *Proceedings of the Institution of Mechanical Engineers, Part E: Journal of Process Mechanical Engineering*, *228*(3), 181–196.

Haddad, Z., Nada, A., Oztop, F., & Mataoui, A. (2012). Natural convection in nanofluids: Are the thermophoresis and Brownian motion effects significant in nanofluid heat transfer enhancement? *International Journal of Thermal Sciences*, *57*, 152.

Hamad, M. A., Pop, I., & Md. Ismail, A. I. (2011). Magnetic field effects on free convection flow of a nanofluid past a vertical semi-infinite flat plate. *Nonlinear Analysis: Real World Application*, *12*, 1338–1346.

Haroun, N. A., Sibanda, P., Mondal, S., & Motsa, S. S. (2015). On unsteady MHD mixed convection in a nanofluid due to a stretching/shrinking surface with suction/injection using the spectral relaxation method. *Boundary Value Problems*, *2015*(1), 24.

Hossain, M. A., & Takhar, H S. (1996). Radiation effect on mixed convection along a vertical plate with uniform surface temperature. *Heat and Mass Transfer*, *31*, 243–248.

Hughes, W. F., & Young, F. J. (1966). *The electromagnetodynamics of fluids*. John Wiley.

Jafar, K., Nazar, R., Ishak, A., & Pop, I. (2011). MHD flow and heat transfer over stretched/shrinking sheets with external magnetic field, viscous dissipation and Joule effects. *Canadian Journal of Chemical Engineering*, *99*, 1–11.

Jumah, R. Y., Banat, F. A., & Abu-Al-Rub, F. (2001). Darcy-Forchheimer mixed convection heat and mass transfer in fluid saturated and porous media. *International Journal of Numerical Methods for Heat and Fluid Flow*, *11*(6), 600–618.

Kang, H. U., Kim, S. H., & Oh, J. M. (2006). Estimation of thermal conductivity of nanofluid using experimental effective particle volume. *Experimental Heat Transfer*, *19*, 181–191.

Keblinski, P., Eastman, J. A., & Cahaill, D. G. (2005). Nanofluids for thermal transport. *Materials Today*, *8*(6), 36.

Khan, M. S., Alam, M. M., & Ferdows, M. (2013). Effects of magnetic field on radiative flow of a nanofluid past a stretching sheet. *Procedia Engineering*, *56*, 316–322.

Liu, M.-S., Lin, M. C.-C., Huang, I.-T., & Wang, C.-C. (2005). Enhancement of thermal conductivity with carbon nanotube for nanofluids. *International Communications in Heat and Mass Transfer*, *32*(9), 1202–1210.

Mabood, F., Khan, W. A., & Ismail, A. I. M. (2015). MHD boundary layer flow and heat transfer of nanofluids over a nonlinear stretching sheet: A numerical study. *Journal of Magnetism and Magnetic Materials*, *374*, 569–576.

Madkour, L. H. (2019). Processing of nanomaterials (NMs). In *Nanoelectronic materials. Advanced structured materials*(Vol. *116*). Springer.

Maiga, S. E. B., Palm, S. J., Nguyen, C. T., Roy, G., & Galanis, N. (2005). Heat transfer enhancement by using nanofluids in forced convection flow. *International Journal of Heat and Fluid Flow*, *26*, 530–546.

Mohammadein, A. A., & El-Amin, M. F. (2000). Thermal radiation effect on power law fluid over a Horizontal plate embedded in a porous medium. *International Communications in Heat and Mass Transfer*, *27*, 1025–1035.

Motsa, S. S. (2014). A new spectral relaxation method for similarity variable nonlinear boundary layer flow systems. *Chemical Engineering Communications*, *201*, 241–256.

Motsa, S. S., & Makukula, Z. G. (2013). On spectral relaxation method approach for steady von Karman flow of a Reiner-Rivlin fluid with Joule heating, viscous dissipation and suction/injection. *Central European Journal of Physics*, *11*(3), 363–374.

Mustafa, M., Khan, J. A., Hayat, T., & Alsaedi, A. (2015). Analytical and numerical solutions for axisymmetric flow of nanofluid due to non-linearly stretching sheet. *International Journal of Non-Linear Mechanics*, *71*, 22–29.

Nadeem, S., Khan, M. N., Muhammad, N., & Ahmad, S. (2019). Mathematical analysis of bio-convective micropolar nanofluid. *Journal of Computational Design and Engineering*, *6*(3), 233–242.

Nadeem, S., Rehman, M. I, Saleem, S., & Bonyah, E. (2020). Dual solutions in MHD stagnation point flow of nanofluid induced by porous stretching/shrinking sheet with anisotropic slip. *AIP Advances*, *10*, 065207.

Oztop, H. F., & Abu-Nada, E. (2008). Numerical study of natural convection in partially heated rectangular enclosures filled with nanofluids. *International Journal of Heat and Fluid Flow*, *29*, 1326–1336.

Rana, P., Bhargava, R., Bég, O. A., & Kadir, A. (2017). Finite element analysis of viscoelastic nanofluid flow with energy dissipation and internal heat source/sink effects. *International Journal of Applied and Computational Mathematics*, *3*(2), 1421–1447.

Downloaded from https://academic.oup.com/jcde/article/8/4/1158/6324282 by University of Salford user on 29 July 2021

Raptis, A. (1998a). Flow of a micropolar fluid past a continuously moving plate by the presence of radiation. *International Journal of Heat and Mass Transfer*, *41*, 2865–2866.

Raptis, A. (1998b). Radiation and free convection flow through a porous medium. *International Communications in Heat and Mass Transfer*, *25*, 289–295.

Rasheed, H., Rehman, A., Sheikh, N., & Iqbal, S. (2017). MHD boundary layer flow of nanofluid over a continuously moving stretching surface. *Applied and Computational Mathematics*, *6*(6), 265–270.

Saleem, S., Qasim, M., Alderremy, A., & Noreen, S. (2020). Heat transfer enhancement using different shapes of Cu nanoparticles in the flow of water based nanofluid, *Physica Scripta*, *95*(5), 055209.

Shateyi, S., & Prakash, J. (2014). A new numerical approach for MHD laminar boundary layer flow and heat transfer of nanofluids over a moving surface in the presence of thermal radiation. *Boundary Value Problems*, *2014*, 2.

Sowmya, G., Gireesha, B. J., & Prasannakumara, B. C. (2019). Scrutinization of different shaped nanoparticle of molybdenum disulfide suspended nanofluid flow over a radial porous fin. *International Journal of Numerical Methods for Heat and Fluid Flow*, *30*(7), 3685–3699. https://doi.org/10.1108/HFF-08-2019-0622.

Srinivasacharya, D., Mendu, U., & Venumadhav, K. (2015). MHD boundary layer flow of a nanofluid past a wedge. *Procedia Engineering*, *127*, 1064–1070.

Thumma, T., Mishra, S. R., & Bég, O. A. (2020). ADM solution for Cu/CuO–water viscoplastic nanofluid transient slip flow from a porous stretching sheet with entropy generation, convective wall temperature and radiative effects. *Journal of Applied and Computational Mechanics*, 1–15. (In press).

Tiwari, R. K., & Das, M. K. (2007). Heat transfer augmentation in a two-sided lid-driven differentially heated square cavity utilizing nanofluids. *International Journal of Heat and Mass Transfer*, *50*, 2002–2018.

Trefethen, L. N. (2000). *Spectral methods in MATLAB*. SIAM.

Tyler, T., Shenderova, O., Cunningham, G., Walsh, J., Drobnik, J., & McGuire, G. (2006). Thermal transport properties of diamond based nanofluids and nanocomposites. *Diamond and Related Materials*, *15*(11–12), 2078–2081.

Tzou, D. Y. (2008). Thermal instability of nanofluids in natural convection. *International Journal of Heat and Mass Transfer*, *51*, 2967–2979.

Uddin, M. J., Bég, O. A., & Ismail, A. I. (2015). Radiative-convective nanofluid flow past a stretching/shrinking sheet with slip effects. *AIAA Journal of Thermophysics and Heat Transfer*, *29*(3), 513–523.

Upreti, H., Pandey, A. K., & Kumar, M. (2020). Thermophoresis and suction/injection roles on free convective MHD flow of Ag–kerosene oil nanofluid. *Journal of Computational Design and Engineering*, *7*(3), 386–396.

Wang, X.-Q., & Mujumdar, A. S. (2007). Heat transfer characteristics of nanofluids: A review. *International Journal of Thermal Sciences*, *46*, 1–19.

Wang, X.-Q., & Mujumdar, A. S. (2008a). A review on nanofluids – Part II: Experiments and applications. *Brazilian Journal of Chemical Engineering*, *25*, 631–648.

Wang, X.-Q., & Mujumdar, A. S. (2008b). A review on nanofluids – Part I: Theoretical and numerical investigations. *Brazilian Journal of Chemical Engineering*, *25*, 613–630.

Yohannes, Y., & Shankar, B. (2014). Melting heat transfer in MHD flow of nanofluids over a permeable exponentially stretching sheet. *Journal of Nanofluids*, *3*, 90–100.

Yu, W., France, D. M., Routbort, J. L., & Choi, S. U. S. (2008). Review and comparison of nanofluid thermal conductivity and heat transfer enhancements. *Heat Transfer Engineering*, *29*(5), 432–460.

Downloaded from https://academic.oup.com/jcde/article/8/4/1158/6324282 by University of Salford user on 29 July 2021